

## Metal Oxide/Gold Hybrid Nanocomposites as Electrocatalysts for Alkaline Air Electrodes

*Anielli M. Pasqualetti, Francisca E. R. Oliveira and Fabio H. B. Lima\**

*Instituto de Química de São Carlos, Universidade de São Paulo, CP 780, 13560-970 São Carlos-SP, Brazil*

MnCo<sub>2</sub>O<sub>4</sub>/Au was investigated as an electrocatalyst for the oxygen reduction and evolution in alkaline media. Polarization curves showed an unprecedented activity for the oxygen reduction due to a synergistic effect between MnCo<sub>2</sub>O<sub>4</sub> and Au, involving Co<sup>II</sup>/Co<sup>III</sup>-Mn<sup>III</sup>/Mn<sup>IV</sup>, as revealed by *in situ* X-ray absorption near edge structure (XANES). Additionally, results showed favorable interaction between the oxide and Au, which enhanced the activity for the oxygen evolution reaction.

**Keywords:** fuel cells, oxygen reduction and evolution, hybrid metal oxide nanocomposites

### Introduction

Fuel cells (FCs) and unitized regenerative fuel cells (URFCs) are interesting energy conversion/storage systems for a sustainable society. An important impulsion for the development of alkaline fuel cells was associated with the recent discovery of the CO<sub>2</sub> self-purging effect, which takes place when they are operated with anion exchange electrolytes and above 80 °C.<sup>1-3</sup> This effect minimizes the problem with the atmospheric CO<sub>2</sub>, and permits long-term operation.

Mn<sub>y</sub>O<sub>x</sub>-based materials usually present high activity for the oxygen reduction reaction (ORR) in alkaline media, but still present high overpotentials.<sup>4-6</sup> On the other hand, the MnCo<sub>2</sub>O<sub>4</sub> spinel oxide results in a more stable and active material.<sup>5</sup> Particularly for URFCs, the difficulty is also related to the choice of a conductive and stable electrocatalyst support. In the case of non-conductive catalysts, such as MnCo<sub>2</sub>O<sub>4</sub>, the electrochemical reaction will not occur over the full surface of the catalyst. It will be constrained to triple phase boundary regions where the oxide makes a contact with a possible conductive phase and the electrolyte. Therefore, it is desirable to increase the surface area of the oxide or of the conductive support in order to enhance the electrocatalytic performance.<sup>7</sup>

In this study, carbon-supported and unsupported MnCo<sub>2</sub>O<sub>4</sub>/Au hybrid nanocomposites were synthesized and investigated as electrocatalysts for the ORR and oxygen evolution reaction (OER). SnO<sub>2</sub>/Au was also prepared in order to separate the contribution of pure Au nanoparticles

(SnO<sub>2</sub> is relatively inactive for these reactions in the investigated potential domains).

### Experimental

The investigated electrocatalysts consisted of MnCo<sub>2</sub>O<sub>4</sub>/C/Au or MnCo<sub>2</sub>O<sub>4</sub>/Au with 20 and 50 wt.% of gold, and 20 wt.% of Mn + Co on carbon (Vulcan XC-72R). MnCo<sub>2</sub>O<sub>4</sub>/C was synthesized according to previous studies.<sup>5,8</sup> Briefly, 132.8 mg of Mn(NO<sub>3</sub>)<sub>2</sub> and 332.8 mg of Co(NO<sub>3</sub>)<sub>2</sub> were dissolved in an aqueous carbon suspension (50 mL of water + 80 mg of carbon, for 100 mg of catalyst), followed by the water evaporation at 80 °C, under magnetic stirring. The dried powder was submitted to a thermal decomposition at 220 °C for 1 h. For the unsupported material, carbon was eliminated by thermal treatment at 900 °C, in air, for 2 h. For the deposition of gold nanoparticles (GNs) on MnCo<sub>2</sub>O<sub>4</sub> or SnO<sub>2</sub> (Sigma-Aldrich, 99.99%, < 100 nm), the oxides (80 or 50 mg) and HAuCl<sub>4</sub> (71.8 or 179.7 µL for 20 or 50 wt.% of gold, respectively) (Sigma-Aldrich) were kept in water (180 mL), and a solution containing 20 mL of water + 5.83 mL of absolute ethanol + 0.82 g of NaOH was dropped into it. This system was maintained under stirring for 2 h and the precipitate was filtered, washed, and dried at 60 °C overnight.

X-Ray diffraction (XRD, RIGAKU Ultima IV diffractometer, Cu K $\alpha$  radiation), X-ray energy dispersive spectrometry (XEDS, Zeiss-Leica/LEO 440 model), transmission electron microscopy (TEM, Jeol GEM 2100, 200 kV), and *in situ* X-ray absorption near edge structure (XANES) (at Laboratório Nacional de Luz Síncrotron (LNLS)) measurements were performed in order to

\*e-mail: fabiohbl@iqsc.usp.br

characterize the materials. The electrochemical experiments were conducted in 1.0 mol L<sup>-1</sup> KOH solution (98.0%); a platinum screen was utilized as counter and Hg/HgO/OH<sup>-</sup> as reference electrodes. The working electrodes were prepared by the deposition of the electrocatalyst ink on a glassy carbon disk of a rotating disk electrode (RDE),<sup>9</sup> followed by the addition of diluted Nafion (0.05 wt.%). Cyclic voltammetry (CV), and polarization curves for ORR, and OER were performed using an AUTOLAB PGSTAT 128N potentiostat.

## Results and Discussion

XRD results (Supplementary Information) showed the tetragonal structure of SnO<sub>2</sub> and the spinel structure of MnCo<sub>2</sub>O<sub>4</sub>, which matched with those of the standard data (Joint Committee on Powder Diffraction Standards (JCPDS)) for these compounds. The average crystallite sizes, calculated by using the Scherrer equation,<sup>10</sup> ( $d = k\lambda / \beta\cos\Theta$ , where  $d$  is the average crystallite size;  $k$  is the shape factor, here 0.9;  $\lambda$  is the X-ray wavelength (Cu K $\alpha$ 1,  $\lambda = 0.15406$  nm);  $\beta$  is the line broadening at half the maximum intensity (in radians);  $\Theta$  is the Bragg angle) resulted in 80.7 and 27.4 nm for MnCo<sub>2</sub>O<sub>4</sub> and SnO<sub>2</sub>, respectively. GNs deposited on MnCo<sub>2</sub>O<sub>4</sub> presented 13.0 and 14.9 nm, and those deposited on SnO<sub>2</sub> presented 20.9 and 22.1 nm, for the loadings of 20 and 50 wt.%, respectively. The composition of gold, determined by XEDS, was ca. 19 and 50 wt.% on MnCo<sub>2</sub>O<sub>4</sub>, which were close to the nominal values; but it was ca. 10 and 30 wt.% on SnO<sub>2</sub>. The differences observed in crystallite sizes and loads of Au on MnCo<sub>2</sub>O<sub>4</sub> and on SnO<sub>2</sub> might be related to distinctive metal-support interactions.

The CVs for the carbon-supported materials (Figure 1a) present anodic and cathodic peaks that become even more evident in the presence of gold. For the pure spinel oxide, the CV is featureless, given that it is a non-conductive material. However, the CV for the MnCo<sub>2</sub>O<sub>4</sub>/Au (Figure 1b) reveals the redox processes from MnCo<sub>2</sub>O<sub>4</sub>, which indicate they can be accessed due to the GNs. Our experiments indicated that the GNs have to touch or be sufficiently close to each other, forming a continuum conductive phase to the surface of the current collector, in order to observe the redox process from the spinel oxide. A similar result was obtained for Pt deposited on Nb-doped SnO<sub>2</sub>.<sup>11</sup> Therefore, GNs may increase electrical conductivity and the redox processes of the spinel oxide can be highlighted.

Figures 2a and 2b show that the XANES main edges of Mn and Co shift to lower values when the electrode potential decreases. The combination of the CVs with the *in situ* XANES results, as well as the comparison between

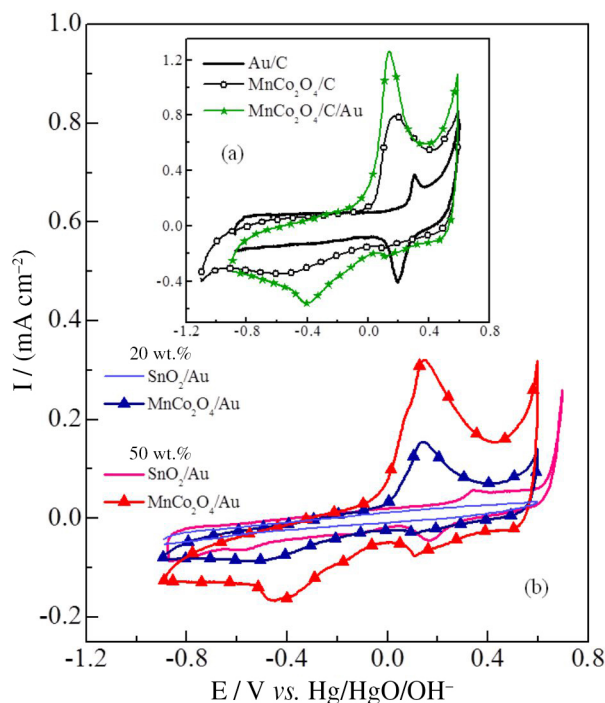


**Figure 1.** (a) CVs for Au/C, MnCo<sub>2</sub>O<sub>4</sub>/C, and MnCo<sub>2</sub>O<sub>4</sub>/C/Au; (b) SnO<sub>2</sub>/Au and MnCo<sub>2</sub>O<sub>4</sub>/Au; 1.0 mol L<sup>-1</sup> N<sub>2</sub>-saturated KOH, at 10 mV s<sup>-1</sup>.

the obtained spectra and those of standard metal oxides, revealed that both Mn and Co change their oxidation state from IV to II.<sup>4,12</sup> Previous results of XPS of Mn<sub>x</sub>Co<sub>3-x</sub>O<sub>4</sub> electrodes indicated that the progressive substitution of Co by Mn atoms in spinel oxide structures increased the Co<sup>2+</sup>/Co<sup>3+</sup> ratio.<sup>13</sup> The *in situ* XANES spectra at the Co edge showed, indeed, the electroreduction to Co<sup>II</sup>, starting at ca. -0.1 V, whereas the Mn edge showed the electroreduction to Mn<sup>III</sup> just below this potential. Therefore, the combination of the CV and XANES results indicates that the anodic current peak at 0.2 V is ascribed to a parallel oxidation from Mn<sup>III</sup> to Mn<sup>IV</sup>, and Co<sup>II</sup> to Co<sup>III</sup> species. The small shoulder at 0.55 V, on the CV, may be related to the oxidation of cobalt species to Co<sup>IV</sup>, although it is difficult to identify the difference between Co<sup>IV</sup> and Co<sup>III</sup> spectra. Accordingly, the small cathodic peak (0.15 V) is related to the reduction to Co<sup>III</sup>, and the broader cathodic peak (from -0.2 to -0.8 V) is associated with a superimposed electroreduction to Co<sup>II</sup> and to Mn<sup>III</sup>, with an additional reduction to Mn<sup>II</sup> at lower potentials.

The ORR on MnCo<sub>2</sub>O<sub>4</sub>/C/Au (Figure 3) presented a high ORR onset potential (similar to that of Au/C, and, interestingly, close to that of Pt/C), and a high ORR limiting current (resembling that of MnCo<sub>2</sub>O<sub>4</sub>/C). Thus, it is proposed the occurrence of a synergistic effect between the metal oxide and the gold nanoparticles. Similarly, the ORR on MnCo<sub>2</sub>O<sub>4</sub>/Au (Figure 4a) presented a gold-like onset potential, and exhibited higher limiting current, owing to the presence of the MnCo<sub>2</sub>O<sub>4</sub>.

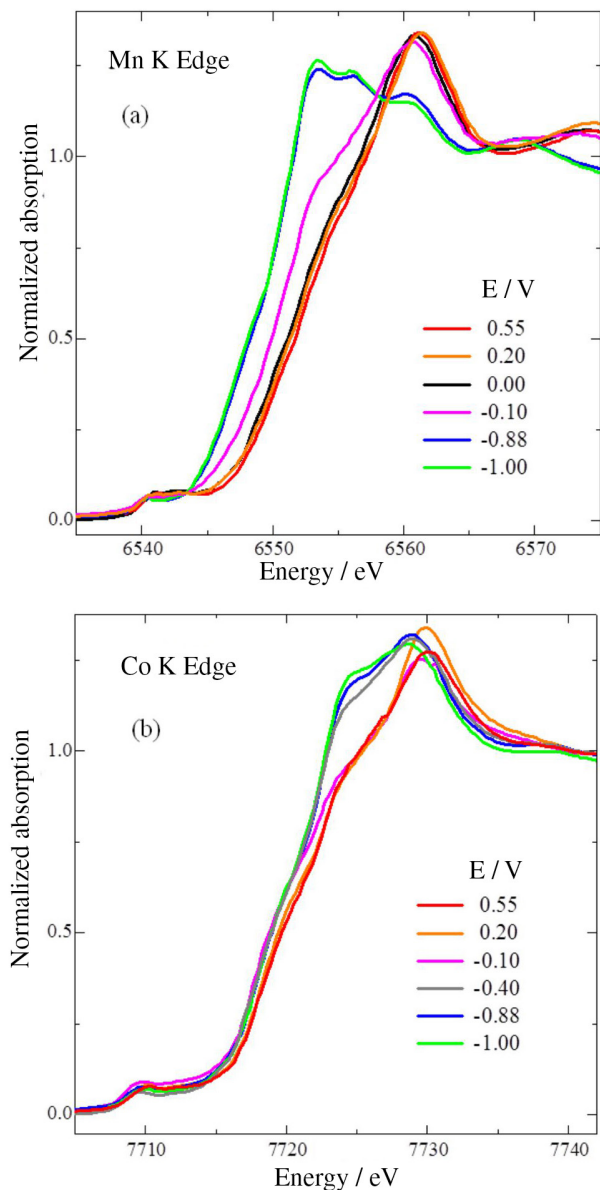


**Figure 2.** *In situ* XANES spectra for  $\text{MnCo}_2\text{O}_4/\text{C}$  at (a) Mn and (b) Co K edges for different potentials in  $1.0 \text{ mol L}^{-1}$  KOH.

Gold presents low oxygen binding energy,<sup>14,15</sup> thus it is hindered to provide 4 electrons during the ORR. On the other hand, the oxide material may produce the O–O bond breaking or the peroxide ion disproportionation.<sup>16</sup> In this case, the ORR on  $\text{MnCo}_2\text{O}_4/\text{Au}$  may initiate on the Au atoms surface, producing peroxide ions, at high potentials. Sequentially, the intermediate species move to the spinel active sites (spillover effect) and react again, following the disproportionation reaction or O–O bond breaking, which increases the number of exchanged electrons per  $\text{O}_2$  molecule. Furthermore, the insertion of Mn into the Co oxide could contribute to reduce  $\text{Co}^{\text{III}}$ , during the ORR, which shows higher electrochemical current than the pure  $\text{Co}_y\text{O}_x/\text{C}$ .<sup>5</sup>

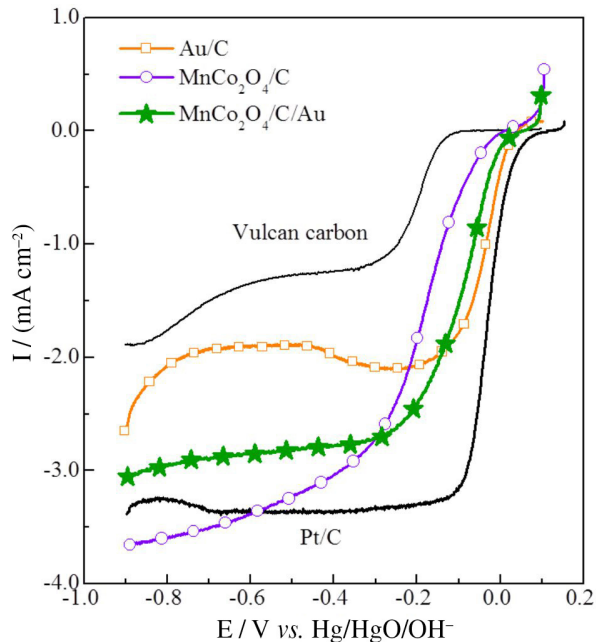


**Figure 3.** ORR (1600 rpm) on Vulcan carbon, Au/C, Pt/C,  $\text{MnCo}_2\text{O}_4/\text{C}$ , and  $\text{MnCo}_2\text{O}_4/\text{C}/\text{Au}$ .  $\text{O}_2$ -saturated  $1.0 \text{ mol L}^{-1}$  KOH, and at  $1 \text{ mV s}^{-1}$ .

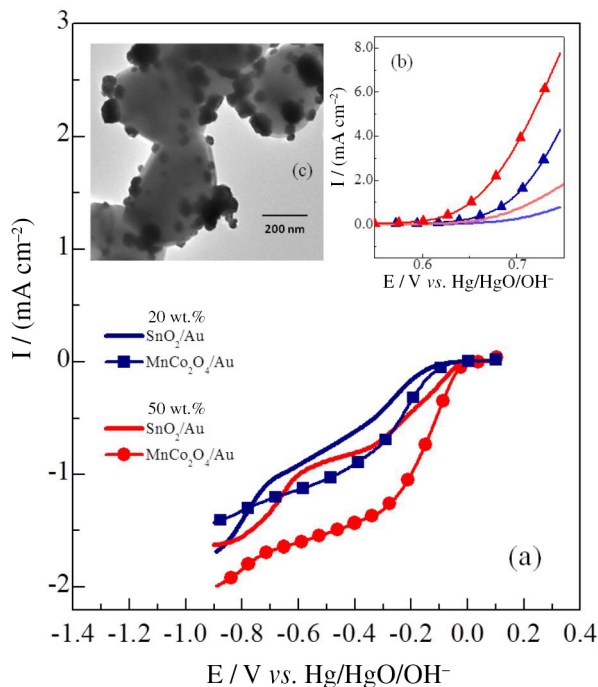


**Figure 4.** (a) ORR at 1600 rpm, and (b) OER on  $\text{SnO}_2/\text{Au}$  and  $\text{MnCo}_2\text{O}_4/\text{Au}$ .  $\text{O}_2$ -saturated  $1.0 \text{ mol L}^{-1}$  KOH, and at  $1 \text{ mV s}^{-1}$ ; (c) TEM image of  $\text{MnCo}_2\text{O}_4/\text{Au}$  with 50 wt.% of gold.

The OER on  $\text{MnCo}_2\text{O}_4/\text{Au}$  presents higher current than  $\text{SnO}_2/\text{Au}$  (Figure 4b,  $\text{SnO}_2$  being inactive), and much higher current than pure  $\text{MnCo}_2\text{O}_4$  (not shown). This evidences that the deposition of GNs is also advantageous for the OER. According to previous studies,<sup>17–19</sup> this increase in activity is associated with (i) change in the OER pathway via the hydrogen acceptor concept<sup>18</sup> or (ii) larger amount of

Co<sup>IV</sup> (OER active species), induced by the presence of Au. The interaction with gold results in more negative values of oxygen binding energy, which facilitates the O–OH bond formation and OOH deprotonation, so enhancing the OER.<sup>19</sup> One can observe in the TEM image of MnCo<sub>2</sub>O<sub>4</sub>/Au with 50 wt.% of Au (Figure 4c), that the gold particles (darker domains) possess a heterogeneous distribution in size. Therefore, further improvements are expected by adopting alternative methods of gold deposition with higher surface area.

## Conclusions

The results showed an unprecedented activity of the MnCo<sub>2</sub>O<sub>4</sub>/Au electrocatalyst for the ORR, with high onset potential and high number of electrons, and this was attributed to the synergistic effect between MnCo<sub>2</sub>O<sub>4</sub> and Au. For the OER, the high activity of the unsupported MnCo<sub>2</sub>O<sub>4</sub>/Au nanocomposite was associated with the hydrogen acceptor concept or an increase in the amount of Co<sup>IV</sup> species, induced by the presence of Au, that are active for the OER.

## Supplementary Information

Supplementary data are available free of charge at <http://jbcs.sbq.org.br> as PDF file.

## Acknowledgments

The authors acknowledge financial support from FAPESP, FHBL (No. 2011/50727-9 and 2013/16930-7), AMP (No. 2013/03408-0); CNPq, FHBL (No. 306213/2013-3); and CAPES. Thanks are due to LNLS for assisting with the XAS experiments.

## References

1. Adams, L. A.; Poynton, S. D.; Tamain, C.; Slade, R. C. T.; Varcoe, J. R.; *ChemSusChem* **2008**, *1*, 79.
2. Fukuta, K.; Inoue, H.; Watanabe, S.; Yanagi, H.; *ECS Trans.*

3. Lang, C. M.; Kim, K.; Kohl, P. A.; *Electrochim. Solid-State Lett.* **2006**, *9*, A545.
4. Lima, F. H. B.; Calegari, M. L.; Ticianelli, E. A.; *Electrochim. Acta* **2007**, *52*, 3732.
5. Queiroz, A. C.; Lima, F. H. B.; *J. Electroanal. Chem.* **2013**, *707*, 142.
6. McBreen, J.; *Electrochim. Acta* **1975**, *20*, 221.
7. Oh, T.; Kim, J. Y.; Shin, Y.; Engelhard, M.; Weil, K. S.; *J. Power Sources* **2011**, *196*, 6099.
8. Nissinen, T.; Leskela, M.; Gasik, M.; Lamminen, J.; *Thermochim. Acta* **2005**, *427*, 155.
9. Schmidt, T. J.; Gasteiger, H. A.; Stab, G. D.; Urban, P. M.; Kolb, D. M.; Behm, R. J.; *J. Electrochem. Soc.* **1998**, *145*, 2354.
10. Cullity, B. D.; Stock, S. R.; *Elements of X-Ray Diffraction*, 3<sup>rd</sup> ed.; Prentice Hall: Upper Saddle River, 2001.
11. Senoo, Y.; Kakinuma, K.; Uchida, M.; Uchida, H.; Deki, S.; Watanabe, M.; *RSC Adv.* **2014**, *4*, 32180.
12. Li, C.; Han, X.; Cheng, F.; Hu, Y.; Chen, C.; Chen, J.; *Nat. Comm.* **2015**, *6*, 7345.
13. Restovic, A.; Rios, E.; Barbato, S.; Ortiz, J.; Gautier, J. L.; *J. Electroanal. Chem.* **2002**, *522*, 141.
14. Nørskov, J. K.; Rossmeisl, J.; Logadottir, A.; Lindqvist, L.; Kitchin, J. R.; Bligaard, T.; Jonsson, H.; *J. Phys. Chem. B* **2004**, *108*, 17886.
15. Christoffersen, E.; Liu, P.; Ruban, A.; Skriver, H. L.; Nørskov, J. K.; *J. Catal.* **2001**, *199*, 123.
16. Mao, L.; Zhang, D.; Sotomura, T.; Nakatsu, K.; Toshiba, N.; Ohsaka, T.; *Electrochim. Acta* **2003**, *48*, 1015.
17. Gorlin, Y.; Chung, C.-J.; Benck, J. D.; Nordlund, D.; Seitz, L.; Weng, T.-C.; Sokaras, D.; Clemens, B. M.; Jaramillo, T. F.; *J. Am. Chem. Soc.* **2014**, *136*, 4929.
18. Frydendal, R.; Busch, M.; Halck, N. B.; Paoli, E. A.; Krtil, P.; Chorkendorff, I.; Rossmeisl, J.; *ChemCatChem* **2015**, *7*, 149.
19. Yeo, B. S.; Bell, A. T.; *J. Am. Chem. Soc.* **2011**, *133*, 5587.

Submitted: July 14, 2015

Published online: September 9, 2015

FAPESP has sponsored the publication of this article.